



Saddle-Node Bifurcation and Vibrational Resonance in a Fractional System with an Asymmetric Bistable Potential

J. H. Yang

*School of Mechatronic Engineering,
China University of Mining and Technology,
Xuzhou, Jiangsu 22116, P. R. China
jianhuayang@cumt.edu.cn*

Miguel A. F. Sanjuán

*Departamento de Física, Universidad Rey Juan Carlos,
Tulipán s/n, 28933 Móstoles, Madrid, Spain
miguel.sanjuan@urjc.es*

F. Tian* and H. F. Yang†

*School of Mechatronic Engineering,
China University of Mining and Technology,
Xuzhou, Jiangsu 22116, P. R. China
*xzkdtf@cumt.edu.cn
†hfyang@cumt.edu.cn*

Received May 22, 2014; Revised September 1, 2014

We investigate the saddle-node bifurcation and vibrational resonance in a fractional system that has an asymmetric bistable potential. Due to the asymmetric nature of the potential function, the response and its amplitude closely depend on the potential well where the motion takes place. And consequently for numerical simulations, the initial condition is a key and important factor. To overcome this technical problem, a method is proposed to calculate the bifurcation and response amplitude numerically. The numerical results are in good agreement with the analytical predictions, indicating the validity of the numerical and theoretical analysis. The results show that the fractional-order of the fractional system induces one saddle-node bifurcation, while the asymmetric parameter associated to the asymmetric nature of the potential function induces two saddle-node bifurcations. When the asymmetric parameter vanishes, the saddle-node bifurcation turns into a pitchfork bifurcation. There are three kinds of vibrational resonance existing in the system. The first one is induced by the high-frequency signal. The second one is induced by the fractional-order. The third one is induced by the asymmetric parameter. We believe that the method and the results shown in this paper might be helpful for the analysis of the response problem of nonlinear dynamical systems.

Keywords: Fractional-order derivative; saddle-node bifurcation; pitchfork bifurcation; vibrational resonance.

*Author for correspondence

1. Introduction

The dynamics of nonlinear dynamical systems with an asymmetric potential has been a topic of interest in the past decades. For example, when an asymmetric bistable system is excited by noise, the first passage time usually needs to be calculated [Wang *et al.*, 2003]. When an asymmetric bistable system is excited by both a noise and a weak signal, the phenomenon of stochastic resonance occurs at an appropriate noise intensity [Xu *et al.*, 2005]. Under a multiscale type excitation, the chaotic behavior in a system with an asymmetric potential has been investigated [Kwuimy *et al.*, 2011]. For a parametric and external harmonic force driven oscillator, the chaotic dynamics of a nonlinear asymmetric oscillator in a plasma device mode has been studied [Buckjohn *et al.*, 2011]. In a Duffing oscillator with asymmetric single-well and double-well potentials, the vibrational resonance has also been investigated by experimental, numerical and analytical methods [Chizhevsky & Giacomelli, 2006; Jeyakumari *et al.*, 2011].

Fractional calculus is a useful tool to model the dynamic property in a wide range of engineering and scientific fields. The fractional-order of a nonlinear system is an important factor to induce complex phenomena. Take the bifurcation in the fractional system as an example, in a fractional Lorenz system, the change of the fractional-order may induce some typical bifurcations such as period-doubling bifurcation, flip bifurcation, tangent bifurcation and interior crisis bifurcation [Sun *et al.*, 2010]. In the nonautonomous logistic system [El-Saka *et al.*, 2009] and the modified hybrid optical system [Abdelouahab *et al.*, 2012], the fractional-order may induce Hopf bifurcation. In the stochastic system, the change of the fractional-order can induce P-bifurcation which makes the stationary probability density function translate from unimodal to bimodal [Chechkin *et al.*, 2003]. In the fractional Duffing system with symmetric bistable potential, the fractional-order of the damping induces pitchfork bifurcation and leads to new vibrational resonance phenomenon [Yang & Zhu, 2012, 2013; Yang *et al.*, 2013].

Vibrational resonance is a phenomenon resulting as the response of nonlinear systems that are excited by both a low-frequency and a high-frequency signal [Landa & McClintock, 2000; Balanaras *et al.*, 2003]. Under this type of excitation, the response amplitude at the low-frequency is a

nonlinear function of the parameter of the high-frequency signal. Specifically, the curve of the response amplitude versus the amplitude or the frequency of the high-frequency signal presents a resonance behavior. The diagram is similar to the typical resonance curve in mechanics. The consequence is that the weak low-frequency signal is excellently enhanced by the high-frequency signal. When the low-frequency harmonic signal is replaced by an aperiodic signal, the vibrational resonance can also be presented [Chizhevsky & Giacomelli, 2008].

To numerically simulate the bifurcation and vibrational resonance phenomenon in an asymmetric system, constitutes a technical problem because the response of a particular nonlinear system depends on the initial condition closely. The dynamical behavior has a striking difference when the motion moves in different potential wells. This leads to the difficulty in verifying the theoretical analysis by the numerical simulations. In the previous literature, although the vibrational resonance and the saddle-node bifurcation are investigated in an asymmetric bistable system [Chizhevsky & Giacomelli, 2006; Jeyakumari *et al.*, 2011], the ways to overcome this difficulty induced by the initial condition in the numerical simulation have not been mentioned. It still constitutes a technical problem. Based on the problems mentioned above, a numerical method will be proposed to simulate the bifurcation and resonance behavior.

Considering a general case, we take a simple fractional oscillator as an example, i.e.

$$\frac{d^\alpha x}{dt^\alpha} = -\frac{dV}{dx} + f \cos(\omega t) + F \cos(\Omega t). \quad (1)$$

The excitations satisfy $f \ll 1$, $\omega \ll \Omega$. The sign α is the fractional-order of the system. Usually, α lies in the range $(0, 2)$. There are several definitions for the fractional derivative, such as the Riemann–Liouville definition, the Caputo definition, the Grünwald–Letnikov definition, etc. [Monje *et al.*, 2010]. Here, we use the Grünwald–Letnikov definition for its widely used and simplicity in the numerical discretization. The Grünwald–Letnikov definition is defined as

$$\left. \frac{d^\alpha x(t)}{dt^\alpha} \right|_{t=kh} = \lim_{h \rightarrow 0} \frac{1}{h^\alpha} \sum_{j=0}^k (-1)^j \binom{\alpha}{j} x(kh - jh), \quad (2)$$

where the binomial coefficients are

$$\begin{aligned} \binom{\alpha}{0} &= 1, \\ \binom{\alpha}{j} &= \frac{\alpha(\alpha-1)\cdots(\alpha-j+1)}{j!}, \quad \text{for } j \geq 1. \end{aligned} \quad (3)$$

The potential function $V(x)$ is

$$V(x) = -\frac{1}{2}\omega_0^2x^2 + \frac{a}{3}x^3 + \frac{b}{4}x^4, \quad (4)$$

with $\omega_0^2, a, b > 0$. The asymmetric property of the potential depends on the parameter a . For the case $a = 0$, the potential has two symmetric wells; while for the case $a \neq 0$, the potential has two asymmetric wells. For the case $a < 0$, the right well is deeper; while for the case $a > 0$, the left well is deeper, as shown in Fig. 1. The parameters ω_0^2 and b mainly influence the width and depth of the potential-well. The roles of width and depth on vibrational resonance are once studied in the ordinary Duffing oscillator [Rajasekar *et al.*, 2010]. Hence, we focus on the effects of α and a on the dynamic behaviors in this paper. The parameters α and a respectively indicate the fractional nature and asymmetric property of the system.

The structure of the paper is organized as follows. In Sec. 2, based on the method of direct partition of motions, the theoretical analysis of the equivalent potential function and the response amplitude are obtained. In Sec. 3, the effects of the fractional-order and the asymmetric parameter on

the saddle-node bifurcation are discussed respectively. In Sec. 4, three kinds of vibrational resonance are studied. Finally, the conclusions of the present paper are given in the last section.

2. Theoretical Analysis

Since the frequencies acting on the system are such that $\omega \ll \Omega$, the method of direction partition of motions can be used to solve the response amplitude at the low-frequency [Blekhman, 2000; Thomsen, 2003]. This method has been used in the theoretical analysis of the Duffing oscillator [Gitterman, 2001; Blekhman & Landa, 2004], the quintic oscillator [Jeyakumari *et al.*, 2009a; Jeyakumari *et al.*, 2009b], the delayed system [Jeevarathinam, 2011], the friction system [Thomsen, 1999], the supported beam [Tcherniak, 1999], the ratchet system [Borromeo & Marchesoni, 2006], the fractional-order system [Yang & Zhu, 2012, 2013], etc. among others. According to this method, we let $x = X + \Psi$, where X and Ψ are a slow motion and a fast motion with periods $2\pi/\omega$ and $2\pi/\Omega$, respectively. Then, Eq. (1) turns into

$$\begin{aligned} \frac{d^\alpha X}{dt^\alpha} + \frac{d^\alpha \Psi}{dt^\alpha} &= \omega_0^2 X + \omega_0^2 \Psi - bX^3 - b\Psi^3 - 3bX^2\Psi \\ &\quad - 3bX\Psi^2 - aX^2 - a\Psi^2 - 2aX\Psi \\ &\quad + f \cos(\omega t) + F \cos(\Omega t). \end{aligned} \quad (5)$$

Searching for the approximate solution of Ψ in the following linear equation

$$\frac{d^\alpha \Psi}{dt^\alpha} = \omega_0^2 \Psi + F \cos(\Omega t), \quad (6)$$

it is easy to obtain

$$\Psi = \frac{F}{\mu} \cos(\Omega t + \varphi), \quad (7)$$

where $\mu^2 = (\Omega^\alpha \cos \frac{\alpha\pi}{2} - \omega_0^2)^2 + (\Omega^\alpha \sin \frac{\alpha\pi}{2})^2$ and $\varphi = -\tan^{-1} \frac{\Omega^\alpha \sin \frac{\alpha\pi}{2}}{\Omega^\alpha \cos \frac{\alpha\pi}{2} - \omega_0^2}$. Substituting Eq. (7) into Eq. (5), and averaging all terms over the range $[0, 2\pi/\Omega]$, we obtain

$$\frac{d^\alpha X}{dt^\alpha} = C_1 X - aX^2 - bX^3 - C_0 + f \cos(\omega t), \quad (8)$$

where $C_1 = \omega_0^2 - \frac{3bF^2}{2\mu^2}$ and $C_0 = \frac{aF^2}{2\mu^2}$. In the averaging process, the slow motion is considered as a constant. In Eq. (8), the effective potential function

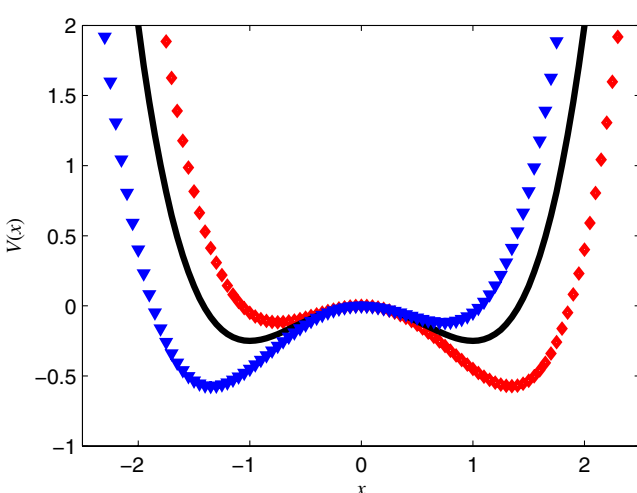


Fig. 1. The shape of the potential function for $\omega_0^2 = 1$, $b = 1$ and $a = -0.6$ (diamonds), 0 (continuous line) and 0.6 (triangles).

of the equivalent system is

$$V_{\text{eff}} = \frac{b}{4}X^4 + \frac{a}{3}X^3 - \frac{C_1}{2}X^2 + C_0X. \quad (9)$$

When the low-frequency excitation is free in Eq. (8), the system may be a bistable system with one unstable equilibrium and two stable equilibria. We designate these three equilibria as X_{S1}^* , X_U^* and X_{S2}^* with $X_{S1}^* < X_U^* < X_{S2}^*$. Here, X_{S1}^* and X_{S2}^* are the stable equilibria while X_U^* is the unstable equilibrium. Or else, Eq. (8) is a monostable system with only one stable equilibrium labeled by X_S^* . The change of the equilibrium is the basis of the local bifurcation analysis.

In general, the slow motion moves around the stable equilibria. Letting, $Y = X - X^{**}$, here X^{**} denotes one stable equilibrium point. X^{**} may equal to X_{S1}^* , or X_{S2}^* , or X_S^* . Then, Eq. (8) turns into

$$\frac{d^\alpha Y}{dt^\alpha} = \omega_r^2 Y - \beta Y^2 - bY^3 + f \cos(\omega t), \quad (10)$$

where $\omega_r^2 = C_1 - 2aX^{**} - 3bX^{**2}$ and $\beta = a + 3bX^{**2}$. According to the linear response theory, the steady response at the excitation frequency can be found in the equation

$$\frac{d^\alpha Y}{dt^\alpha} = \omega_r^2 Y + f \cos(\omega t). \quad (11)$$

Ignoring the transient induced by the initial perturbation, the steady solution of Eq. (11) is $Y = A_L \cos(\omega t + \theta)$, where

$$\left\{ \begin{array}{l} A_L = \frac{f}{\sqrt{\left(\omega^\alpha \cos \frac{\alpha\pi}{2} - \omega_r^2\right)^2 + \left(\omega^\alpha \sin \frac{\alpha\pi}{2}\right)^2}} \\ \theta = -\tan^{-1} \frac{\omega^\alpha \sin \frac{\alpha\pi}{2}}{\omega^\alpha \cos \frac{\alpha\pi}{2} - \omega_r^2} \end{array} \right. \quad (12)$$

Usually, we are interested in the quality of the signal enhancement of a system. Hence, a quantitative index called response amplitude is defined as

$$\begin{aligned} Q &= \frac{A_L}{f} \\ &= \frac{1}{\sqrt{\left(\omega^\alpha \cos \frac{\alpha\pi}{2} - \omega_r^2\right)^2 + \left(\omega^\alpha \sin \frac{\alpha\pi}{2}\right)^2}}. \end{aligned} \quad (13)$$

Obviously, Q measures the degree of enhancement of the weak signal after passing through the nonlinear system. On the basis of Q , the resonance phenomenon can be analyzed. When the denominator has the minimal value, the resonance occurs.

3. Saddle-Node Bifurcation

The saddle-node bifurcation is determined by the real equilibria of Eq. (8), i.e. the roots of the equation

$$C_1X - aX^2 - bX^3 - C_0 = 0. \quad (14)$$

With the change of the bifurcation parameter, the saddle-node bifurcation occurs when two equilibria coalesce and appear/disappear [Guckenheimer & Holmes, 1983; Medio & Lines, 2001]. In previous literature [Jeyakumari et al., 2011], the saddle-node bifurcation induced by the amplitude of the high-frequency signal was discussed analytically. In this section, we will study the effects of the fractional-order α and the asymmetric parameter a on the saddle-node bifurcation. A numerical method is proposed to determine the bifurcation point.

3.1. Effect of the fractional-order on the bifurcation

The bifurcation induced by the fractional-order α is given in Fig. 2. When $a \neq 0$, as shown in Figs. 2(a) and 2(c), a saddle-node bifurcation occurs. For the case $a < 0$, there is always a positive stable branch. Before the bifurcation, this stable branch is constituted by the sole stable equilibrium points X_S^* . When α crosses the bifurcation point, an unstable branch and a negative stable branch appear simultaneously. Meanwhile, the sole stable equilibrium point X_S^* turns into the stable equilibrium point X_{S2}^* . While for the case $a > 0$, a negative stable branch is always existing. With the increase of α , an unstable branch and a positive stable branch appear simultaneously. When α crosses the bifurcation point, the sole stable equilibrium point X_S^* turns into the stable equilibrium point X_{S1}^* for this case. In Fig. 2, the critical value for the saddle-node bifurcation is $\alpha = 0.96$ for both $a = 0.6$ and $a = -0.6$. The critical value of α at the saddle-node bifurcation point is influenced by the quantity, but not the sign of the asymmetric parameter a . In Fig. 2(b), $a = 0$, the potential is symmetric. For this case, the bifurcation induced by the

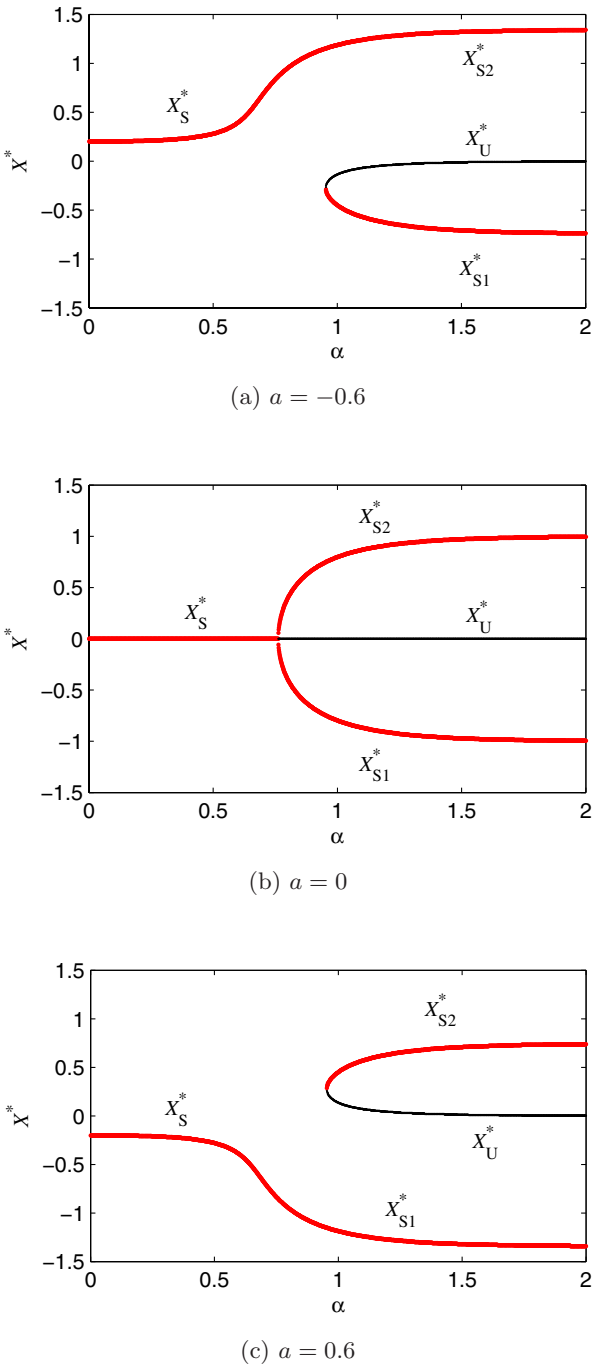


Fig. 2. Analytical prediction of the fractional-order induced bifurcation for $\omega_0^2 = 1$, $b = 1$, $F = 3$ and $\Omega = 6$. In (a) and (c), the saddle-node bifurcation appears. In (b), the pitchfork bifurcation appears.

fractional-order is a supercritical pitchfork bifurcation. Besides the supercritical pitchfork in this subplot, the supercritical pitchfork bifurcation induced by the high-frequency and the subcritical pitchfork bifurcation induced by the amplitude of the high-frequency signal were discussed in detail in a

previous paper [Yang *et al.*, 2013]. Here, we are only interested in the bifurcation induced by the fractional-order. Certainly, the bifurcation induced by the high-frequency signal can also be investigated by the same method. It is worth noting that the bifurcation behavior in Figs. 2(a) and 2(c) is named as perturbed pitchfork bifurcation by Thomassen [2003]. The term $\frac{a}{3}x^3$ in the original potential function in Eq. (4) is regarded as a perturbation. It causes qualitative changes to the pitchfork bifurcation diagram. In other words, the supercritical pitchfork bifurcation is unstable to the asymmetric parameter a . Hence, the perturbation term takes the bifurcation away from the pitchfork. Notice that, the saddle-node bifurcation is generic, whereas the pitchfork bifurcation is not. Besides, the saddle-node bifurcation is discontinuous but the pitchfork bifurcation is continuous. The pitchfork bifurcation occurs with the appearance/disappearance of the equilibrium points and their stability changes at the same time. Apparently, in Figs. 2(a) and 2(c) the stability of one stable branch does not change after crossing the bifurcation point. Specifically, a stable branch is always in a stable state when α lies in $(0, 2)$. As a result, the bifurcation in Figs. 2(a) and 2(c) is a saddle-node bifurcation, but not a pitchfork bifurcation.

In order to verify the validity of the analytical prediction of the bifurcation behavior, the numerical simulation should be carried out. If there is no cross-well motion occurring between the two wells, the equilibrium point around which the motion takes place depends on the initial conditions. According to Eq. (13), it further influences the value of the response amplitude. Only to make this problem clear, the analytical predictions of the bifurcation behavior in Fig. 2 and the response amplitude in Eq. (13) can be verified by the numerical simulation correctly. The time series calculated from Eq. (1) under different initial conditions are given in Fig. 3. For the case $\alpha = 0.5$, the four paths coincide completely after a very short time. The motion occurs around the only stable equilibrium X_S^* . For the case $\alpha = 1.5$, there are two paths moving around the equilibrium X_{S1}^* and two others moving around the equilibrium X_{S2}^* . After the transient motion, the time series along the same manifold are completely coincident. According to this fact, for different initial conditions, the motions are only located in one or two specific locations after a long enough time interval. In the simulation, only

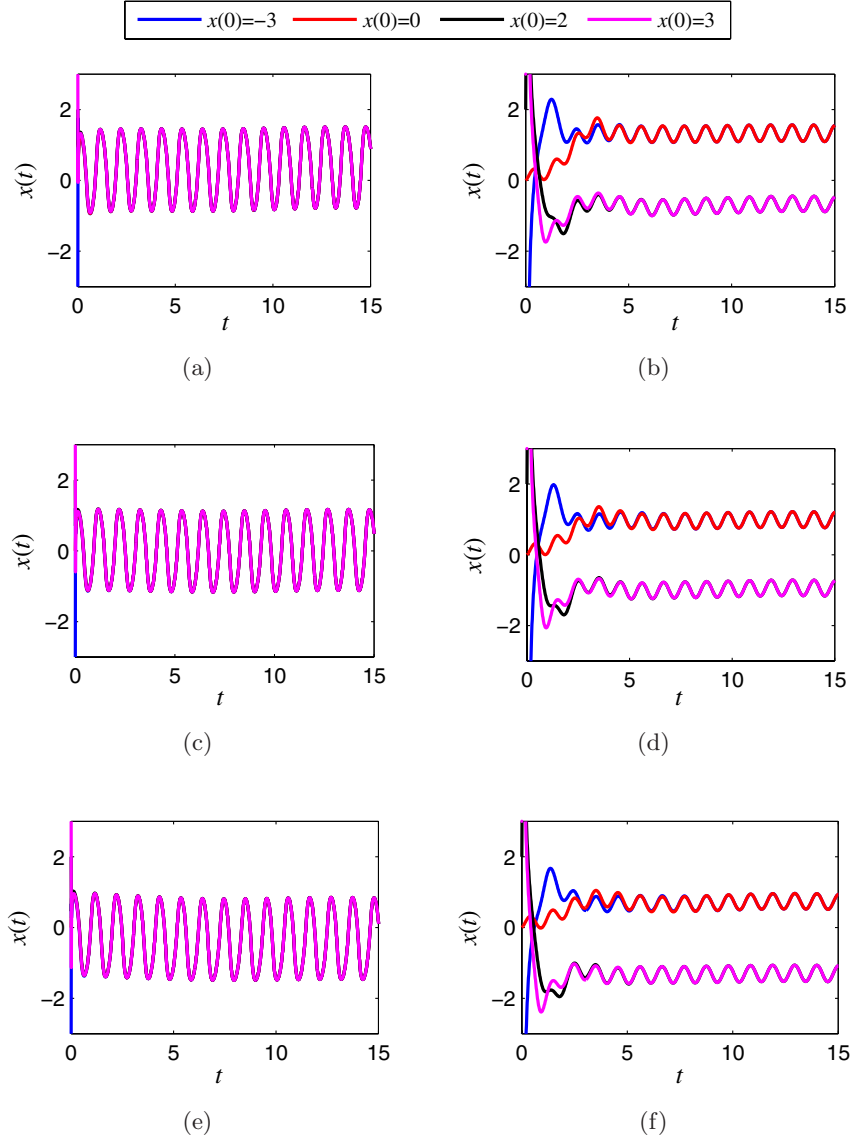


Fig. 3. Time series under different initial conditions for $f = 0.05$, $\omega_1 = 0.5$, $F = 3$, $\Omega = 6$. In (a) and (b), $a = -0.6$; in (c) and (d), $a = 0$; in (e) and (f), $a = 0.6$. In (a), (c) and (e), $\alpha = 0.5$; In (b), (d) and (f), $\alpha = 1.5$.

the steady time series around the stable equilibrium appear. As a result, at a fixed time, there are two specific locations if the system has two stable equilibria, no matter how many series we consider. However, the amplitude of the response at a specific frequency may be different when the motion takes place in different wells.

Based on the fact described in Fig. 3, a numerical method is proposed to predict the bifurcation shown in Fig. 2. The detailed step to carry out the numerical simulation of the bifurcation behavior is as follows. First, we choose every point in the interval $-3:0.06:3$ as the initial condition $x(0)$, where -3 and 3 are the beginning point and end point of the interval respectively, and 0.06 is the step.

Then, we mark the location at the time $10T$, here $T = 2\pi/\omega$. In Fig. 4, the fractional-order induced bifurcation is shown through numerical simulations. The saddle-node bifurcation is shown in Figs. 4(a) and 4(c), and the pitchfork bifurcation is shown in Fig. 4(b). The critical value of the bifurcation is $\alpha = 0.97, 0.75$ and 0.97 for the case $a = -0.6, 0$ and 0.6 respectively. For the analytical results in Fig. 2, the corresponding bifurcation point is $\alpha = 0.96, 0.76$ and 0.96 . The figure shows that the numerical results are in good agreement with the analytical results. It also proves the validity of the analytical and numerical methods that were used above. Both in Figs. 2 and 4, for the saddle-node bifurcation, we always have the first stable branch. The

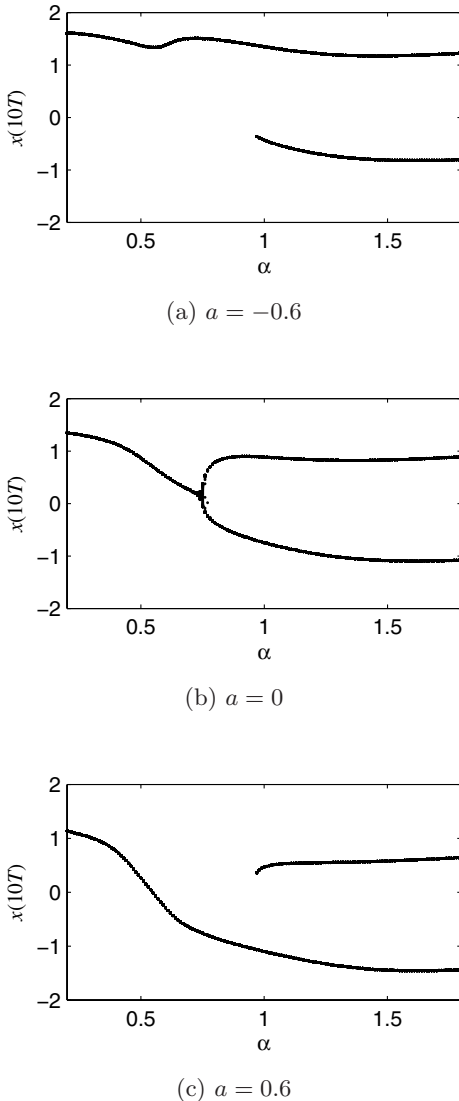


Fig. 4. Numerical prediction of the fractional-order induced bifurcation for α for $\omega_0^2 = 1$, $b = 1$, $f = 0.05$, $\omega = 0.5$, $F = 3$ and $\Omega = 6$. In (a) and (c), the saddle-node bifurcation appears. In (b), the pitchfork bifurcation appears. The initial condition for each numerical simulation is one point in the interval $-3:0.06:3$.

second stable branch appears after the bifurcation point. While for the supercritical pitchfork bifurcation, the first stable branch splits into two stable branches, then they break away gradually. The numerical bifurcation diagrams prove the discontinuity of the saddle-node bifurcation and the continuity of the pitchfork bifurcation again. The idea of the numerical method in this paragraph is also applied to calculate the safe basin in the nonlinear system [Lenci & Rega, 2003; Shang & Xu, 2009]. Certainly, one reason to use this method lies in the periodic or quasiperiodic property of the time series

response. If the time series is chaotic, the method may be not valid. As is well known, for chaotic time series, the locations of different paths at a certain time are distributed almost in a random manner.

3.2. Role of the asymmetric parameter on the bifurcation

The analytical prediction of the saddle-node bifurcation induced by the asymmetric parameter a is given in Fig. 5. There are two saddle-node bifurcation points in the figure. The first saddle-node bifurcation point appears at $a = -0.21$, while the second one appears at $a = 0.21$. Specifically, when the asymmetric parameter a lies in $[-0.21, 0.21]$, the system has two stable branches constituted by the equilibrium points X_{S1}^* and X_{S2}^* respectively. When a lies in other intervals, the system only has one stable branch constituted by the equilibrium points X_S^* . The diagram is symmetric about the line $X^* = 0$. In this figure, with the increase of the asymmetric parameter from negative to positive, the first bifurcation point is the beginning point of a stable branch and an unstable branch. The second bifurcation point is the end point of a stable branch and an unstable branch. For the first saddle-node bifurcation, an additional stable branch appears after the bifurcation point. Hence, we consider the first bifurcation as the supercritical case. Similarly, we think the second saddle-node bifurcation as the subcritical case because an additional stable branch exists before the second bifurcation point. The numerical prediction of the saddle-node

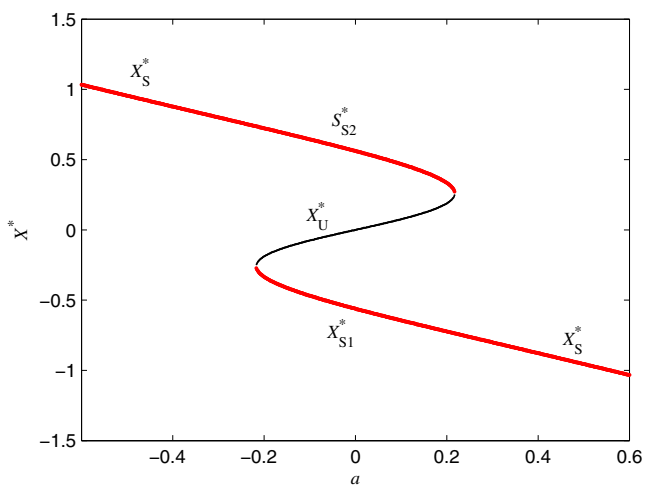


Fig. 5. Analytical prediction of the asymmetric parameter induced saddle-node bifurcation for $\alpha = 1.1$, $\omega_0^2 = 1$, $b = 1$, $f = 0.05$, $\omega = 0.5$, $F = 5$ and $\Omega = 6$.

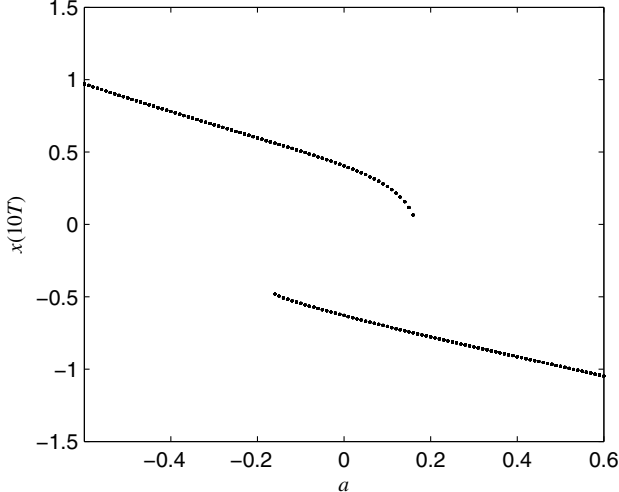


Fig. 6. Numerical prediction of the asymmetric parameter induced saddle-node bifurcation for $\alpha = 1.1$, $\omega_0^2 = 1$, $b = 1$, $f = 0.05$, $\omega = 0.5$, $F = 5$ and $\Omega = 6$. The initial condition for each numerical simulation is one point in the interval $-3:0.06:3$.

bifurcation induced by the asymmetric parameter a is shown in Fig. 6. For the numerical results, the first saddle-node bifurcation point appears at $a = -0.16$ and the second one appears at $a = 0.16$. In this figure, the numerical calculations are also in good agreement with the analytical results, proving the validity of the numerical method again.

4. Three Kinds of Vibrational Resonance

The vibrational resonance induced by the high-frequency signal is the common vibrational resonance [Landa & McClintock, 2000]. It resembles the common resonance phenomenon known in mechanics. Here, we analyze three kinds of vibrational resonance: the vibrational resonance induced by the high-frequency signal, the asymmetric parameter and the fractional-order. For numerical simulation, the response amplitude Q is calculated by the following formula, i.e.

$$Q = \frac{\sqrt{Q_{\sin}^2 + Q_{\cos}^2}}{f}, \quad (15)$$

where

$$\begin{aligned} Q_{\sin} &= \frac{2}{rT} \int_0^{rT} x(t) \sin(\omega t) dt, \\ Q_{\cos} &= \frac{2}{rT} \int_0^{rT} x(t) \cos(\omega t) dt. \end{aligned} \quad (16)$$

Herein, $T = 2\pi/\omega$ and r is a positive integer which should be chosen big enough. In the following simulations, the total time is $200T$. After removing the first $100T$ as the transient response, we make the last $100T$ as the steady response for computation. The time step is $\Delta t = 0.01$.

4.1. Vibrational resonance induced by the high-frequency signal

In Fig. 7, the vibrational resonance induced by the high-frequency signal is shown for different simulation parameters. The double-resonance is shown in Figs. 7(a) and 7(f), and the single-resonance is shown in other subplots of Fig. 7. If the equivalent system in Eq. (8) has two stable equilibria, we substitute $X^{**} = X_{S1}^*$ into Eq. (13) to obtain Figs. 7(a), 7(c), 7(e), and we substitute $X^{**} = X_{S2}^*$ into Eq. (11) to obtain Figs. 7(b), 7(d), 7(f). Or else, we substitute the only stable state $X^{**} = X_S^*$ into Eq. (13) to obtain the analytical result of the response amplitude. Apparently, the analytical curve in Fig. 7(a) is the same with the one in Fig. 7(f). The analytical curve in Fig. 7(b) is consistent with that in Fig. 7(e). The two analytical curves in Figs. 7(c) and 7(d) are completely identical. For numerical simulations, we let $x(0) = -1.5$ in Figs. 7(a), 7(c), 7(e) and $x(0) = 1.5$ in Figs. 7(b), 7(d), 7(f). In fact, it is difficult to assure that the motion occurs always around the stable equilibrium $X^{**} = X_{S1}^*$ or $X^{**} = X_S^*$ in Figs. 7(a), 7(c), 7(e) and around the stable equilibrium $X^{**} = X_{S2}^*$ or $X^{**} = X_S^*$ in Figs. 7(b), 7(d), 7(f). In Fig. 7, the numerical results equal the analytical results approximately. One factor leading to the discrepancy between the analytical results and the numerical simulations is due to the Grünwald–Letnikov algorithm being a crude numerical method [Oldham & Spanier, 2002]. Especially when α is small, the discrepancy is slightly big. However, the errors between the two kinds of results are in an allowable range.

In Fig. 8, the vibrational resonance phenomenon, the usual one, i.e. induced by the biharmonic periodic driving of different frequencies, is shown for the case $\alpha = 1.5$. To obtain the analytical plots in Figs. 8(a), 8(c), 8(e), we suppose that the motion is taking place around the left stable equilibrium X_{S1}^* when there are two stable equilibria or around the sole stable equilibrium X_S^* when there is only one stable equilibrium. To obtain the analytical plots in Figs. 8(b), 8(d), 8(f), we suppose

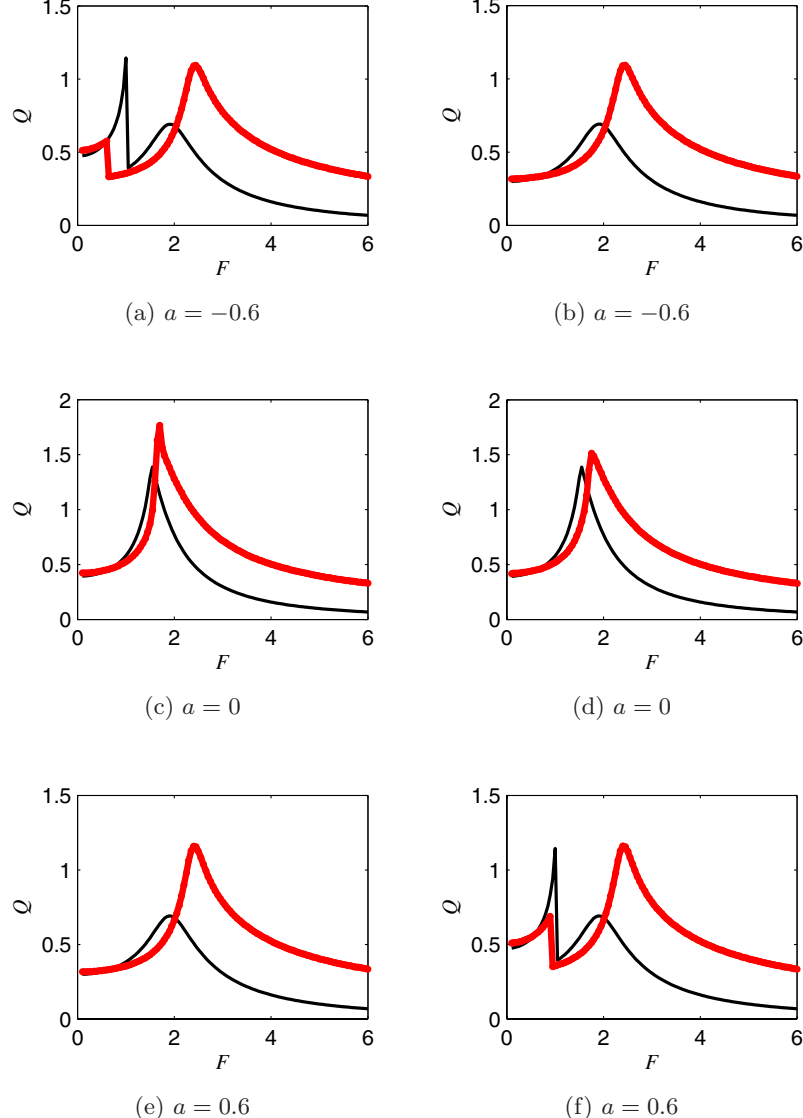


Fig. 7. Vibrational resonance induced by the high-frequency signal for $\alpha = 0.5$, $\omega_0^2 = 1$, $b = 1$, $f = 0.05$, $\omega = 0.5$ and $\Omega = 6$. In (a), (c), (e), $x(0) = -1.5$; in (b), (d), (f), $x(0) = 1.5$. The thin lines are the analytical predictions while the thick lines are the corresponding numerical results.

that the motion takes place around the right stable equilibrium X_{S2}^* or around the sole stable equilibrium X_S^* . The agreement of the numerical simulations with the analytical results proves this fact. The figure also indicates the dependency of the response amplitude on the initial condition. This is due to the fact that the initial condition is a key factor to determine the potential well where the motion takes place. The depths of the two potentials are different for the asymmetric potential case. This explains the difference in the response amplitude when the motions occur in different potential wells. The importance of the initial condition on the response is shown in both Figs. 7 and 8.

Hence, in the asymmetric system, we need a method to determine in which potential well the motion is located in, before we calculate the response amplitude correctly.

4.2. Vibrational resonance induced by the fractional-order

In Fig. 9, we see that the response amplitude is a nonlinear function of the fractional-order α . In this figure, the bold line is obtained by analytical predictions under the precondition that the motion takes place around the stable equilibrium X_{S1}^* or around the sole stable equilibrium X_S^* . The

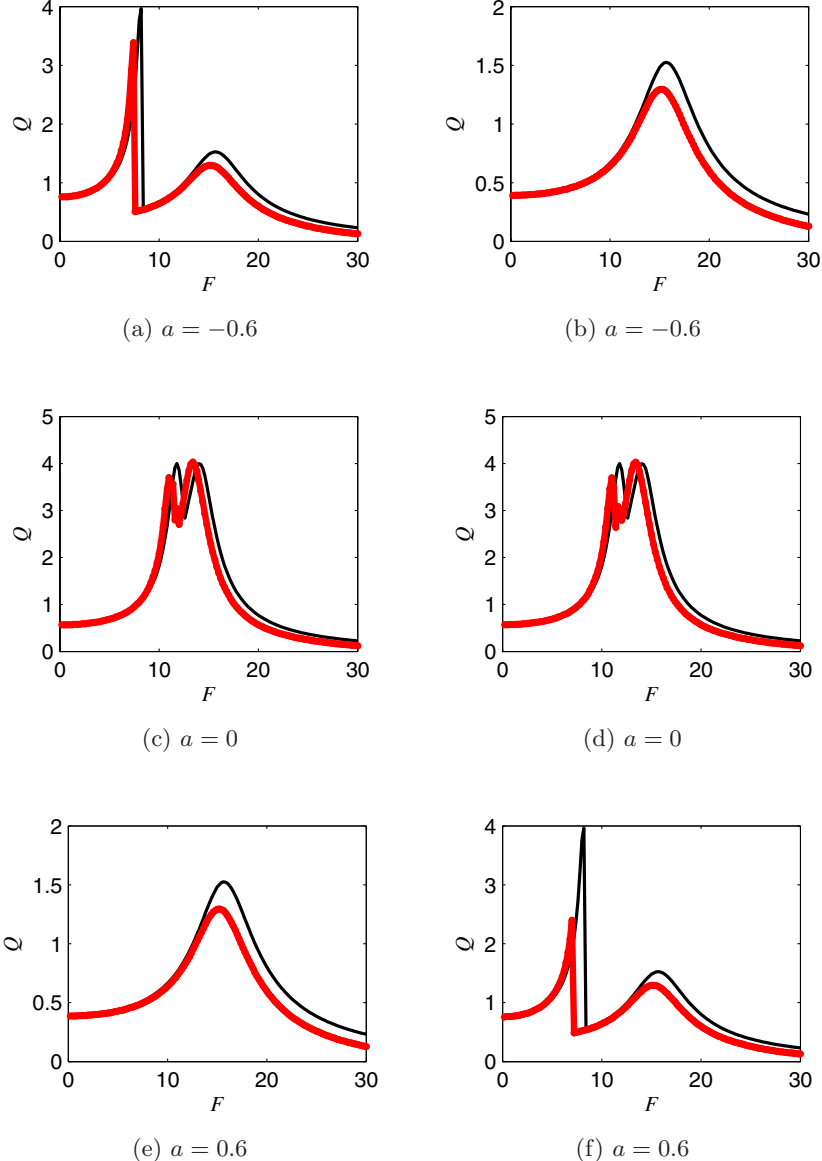


Fig. 8. Vibrational resonance induced by the high-frequency signal for $\alpha = 1.5$, $\omega_0^2 = 1$, $b = 1$, $f = 0.05$, $\omega = 0.5$ and $\Omega = 6$. In (a), (c), (e), $x(0) = 3$; in (b), (d), (f), $x(0) = -3$. The thin lines are analytical predictions while the thick lines are the corresponding numerical results.

line with circles is obtained under the precondition that the motion occurs around the stable equilibrium X_{S2}^* or around the sole stable equilibrium X_S^* . When α is treated as a controllable parameter, for numerical calculations under different initial conditions, it is very difficult to determine in which potential well the motion is taking place. This leads to the difficulty in verifying the analytical results by the numerical simulations. To overcome this problem, we take the method that we have used to calculate the bifurcation in Sec. 3. Specifically, we take one point in the interval $-3:0.06:3$ as the initial location $x(0)$ for each numerical simulation.

Among all different paths, some move around the left equilibrium point and others move around the right equilibrium point when there are two stable equilibrium points. Or else, the motions are around the sole stable equilibrium point. In a short time, the paths that move around the same equilibria achieve a complete synchronization state. Moreover, the coincident paths have the same amplitude in the response series. Hence, it is feasible to numerically simulate the vibrational resonance under different initial conditions. In Fig. 9(a), for the case $a = -0.6$, the double-resonance occurs when the motion takes place around the left equilibrium X_{S1}^*

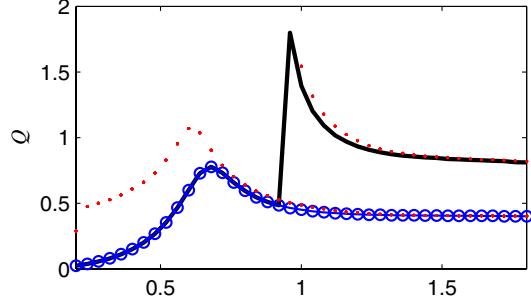
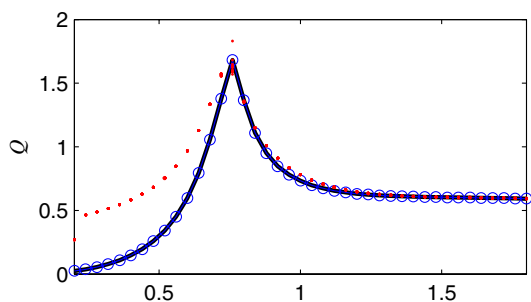
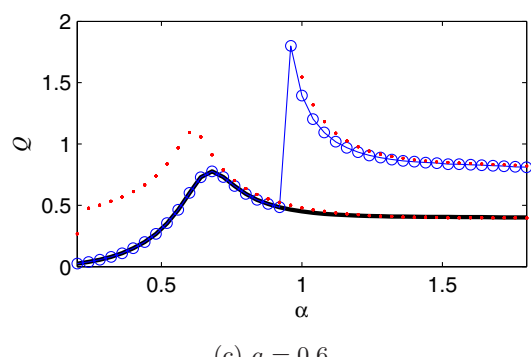
(a) $a = -0.6$ (b) $a = 0$ (c) $a = 0.6$

Fig. 9. Vibrational resonance induced by the fractional-order α for $\omega_0^2 = 1$, $b = 1$, $f = 0.05$, $\omega = 0.5$ and $\Omega = 6$. The bold line and the line with circles are obtained by the analytical predictions while the discrete points are the corresponding numerical results. The initial condition for each numerical simulation is one point in the interval $-3:0.06:3$.

or around the sole stable equilibrium X_S^* while the single-resonance appears when the motion is around the right equilibrium X_{S2}^* or around the sole stable equilibrium X_S^* . In Fig. 9(b), for the case $a = 0$, the potential is symmetric and the curve only has a single peak. In Fig. 9(c), for the case $a = 0.6$, the double-resonance occurs when the motion occurs around the right equilibrium X_{S2}^* or around the sole stable equilibrium X_S^* , while

the single-resonance appears when the motion is around the left equilibrium X_{S1}^* or around the sole stable equilibrium X_S^* . In Fig. 9, the asymmetric parameter a results in the double-resonance occurring in the $Q-\alpha$ plot. Furthermore, another prediction for the double-resonance occurring in Fig. 9 is that the motion should be in the shallow potential well. This subsection shows that the vibrational resonance also appears when the excitation is fixed and the fractional-order is varying.

4.3. Vibrational resonance induced by the asymmetric parameter

The parameter-induced stochastic resonance is known to occur in nonlinear systems [Duan & Xu, 2003]. Since vibrational resonance is a similar phenomenon, one may wonder whether vibrational resonance might also be induced by changing a parameter in a nonlinear system. The answer is given in Fig. 10. In this figure, the bold line is obtained by analytical predictions under the precondition that the motion takes place around the stable equilibrium X_{S1}^* or around the sole stable equilibrium X_S^* . The line with circles is obtained by analytical predictions under the precondition that the motion occurs around the stable equilibrium X_{S2}^* or around the sole stable equilibrium X_S^* . When the asymmetric parameter a increases from negative to positive, the vibrational resonance occurs, no matter around which stable equilibrium

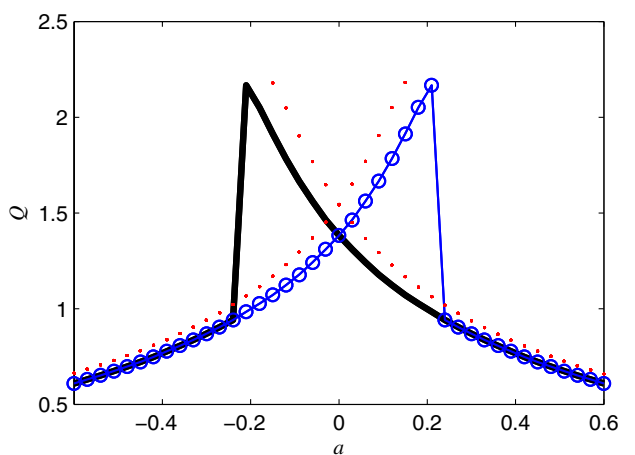


Fig. 10. Vibrational resonance induced by the asymmetric parameter a for $\alpha = 1.1$, $\omega_0^2 = 1$, $b = 1$, $f = 0.05$, $\omega = 0.5$, $F = 5$ and $\Omega = 6$. The bold line and the line with circles are obtained by the analytical predictions while the discrete points are the corresponding numerical results. The initial condition for each numerical simulation is one point in the interval $-3:0.06:3$.

the motion takes place. The two diagrams of the response amplitude are symmetric about the line $a = 0$. The resonance occurs at the point $a = -0.21$ (analytical result), $a = -0.16$ (numerical result), $a = 0.16$ (numerical result) and $a = 0.21$ (analytical result), when the motion occurs around different equilibria. Moreover, from Figs. 5 and 6, we know that these values of a are just the critical points of the saddle-node bifurcation. Therefore, the resonance occurs at the bifurcation point. A detailed discussion of the resonance condition in a fractional system can be found in [Yang & Zhu, 2012]. From our previous work, we know that only when the denominator in Eq. (13), i.e. $\sqrt{(\omega^\alpha \cos \frac{\alpha\pi}{2} - \omega_r^2)^2 + (\omega^\alpha \cos \frac{\alpha\pi}{2})^2} = 0$, does not have a real root, then the single-resonance behavior appears as shown in Fig. 10. From Fig. 10, we also know that the vibrational resonance can be induced by the asymmetric parameter in a fractional system under fixed excitations.

5. Conclusions

The saddle-node bifurcation and vibrational resonance are investigated in a fractional system which has an asymmetric bistable potential. The bifurcation and resonance can be predicted by the analytical and numerical analysis. For numerical simulations, the time series closely depends on the initial condition. To solve this technical problem, a method is proposed to investigate the bifurcation and resonance phenomenon. Specifically, we choose a series of initial conditions which make the response realize all possible paths. If so, on the one hand, all possible locations can be reached at a fixed time. Based on this idea, we analyze the bifurcation. On the other hand, all time series simulated under different initial conditions can achieve all possible response amplitudes. Hence, the vibrational resonance is numerically calculated in an effective manner. The numerical results are in good agreement with the analytical ones, proving the validity of the analytical and numerical analysis.

If the fractional-order is a controllable parameter, the fractional-order induces a saddle-node bifurcation when the asymmetric parameter exists. The fractional-order induces a supercritical pitchfork bifurcation when the asymmetric parameter vanishes. If the asymmetric parameter is treated as a variable, there might exist two saddle-node bifurcations. The first bifurcation point and the second bifurcation point are symmetric around the

origin. The first saddle-node bifurcation occurs behind the bifurcation point. It is a supercritical case. The second saddle-node bifurcation occurs before the bifurcation point. It is a subcritical case.

The response amplitude of the output depends on which potential well the motion takes place. It arises from the asymmetric property of the potential function. There are three kinds of vibrational resonance in the fractional system. The first one is induced by the high-frequency signal. The second one is induced by the fractional-order. The third one is induced by the asymmetric parameter. Hence, we have three ways to make the vibrational resonance to occur in the fractional system. Moreover, the numerical method proposed in this paper might be useful in studying the bifurcation phenomena in nonlinear systems.

Acknowledgments

We acknowledge financial supports by the National Natural Science Foundation of China (Grant No. 51305441), the China Postdoctoral Science Foundation (Grant No. 2012M510192), the Natural Science Foundation of Jiangsu Province (Grant No. BK2011218), the Priority Academic Program Development of Jiangsu Higher Education Institutions, the Spanish Ministry of Science and Innovation (Grant No. FIS2009-09898) and the Spanish Ministry of Economy and Competitiveness (Grant No. FIS2013-40653-P).

References

- Abdelouahab, M. S., Hamri, N. E. & Wang, J. [2012] "Hopf bifurcation and chaos in fractional-order modified hybrid optical system," *Nonlin. Dyn.* **69**, 275–284.
- Baltanas, J. P., Lopez, L., Blechman, I. I., Landa, P. S., Zaikin, A., Kurths, J. & Sanjuán, M. A. F. [2003] "Experimental evidence, numerics, and theory of vibrational resonance in bistable systems," *Phys. Rev. E* **67**, 066119-1–7.
- Blekhman, I. I. [2000] *Vibrational Mechanics: Nonlinear Dynamic Effects, General Approach, Applications* (World Scientific, Singapore).
- Blekhman, I. I. & Landa, P. S. [2004] "Conjugate resonances and bifurcations in nonlinear systems under biharmonical excitation," *Int. J. Nonlin. Mech.* **39**, 421–426.
- Borromeo, M. & Marchesoni, F. [2006] "Vibrational ratchets," *Phys. Rev. E* **73**, 016142-1–8.
- Buckjohn, C. N. D., Siewe, M. S., Tchawoua, C. & Kofan, T. C. [2011] "Transition to chaos in plasma density

- with asymmetry double-well potential for parametric and external harmonic oscillations," *Int. J. Bifurcation and Chaos* **21**, 1879–1893.
- Chechkin, A. V., Klafter, J., Gonchar, V. Y., Metzler, R. & Tanatarov, L. V. [2003] "Bifurcation, bimodality, and finite variance in confined Lévy flights," *Phys. Rev. E* **67**, 010102(R)-1–4.
- Chizhevsky, V. N. & Giacomelli, G. [2006] "Experimental and theoretical study of vibrational resonance in a bistable system with asymmetry," *Phys. Rev. E* **73**, 022103-1–4.
- Chizhevsky, V. N. & Giacomelli, G. [2008] "Vibrational resonance and the detection of aperiodic binary signals," *Phys. Rev. E* **77**, 051126-1–7.
- Duan, F. & Xu, B. [2003] "Parameter-induced stochastic resonance and baseband binary PAM signals transmission over an AWGN channel," *Int. J. Bifurcation and Chaos* **13**, 411–425.
- El-Saka, H. A., Ahmed, E., Shehata, M. I. & El-Sayed, A. M. A. [2009] "On stability, persistence, and Hopf bifurcation in fractional order dynamical systems," *Nonlin. Dyn.* **56**, 121–126.
- Gitterman, M. [2001] "Bistable oscillator driven by two periodic fields," *J. Phys. A: Math. Gen.* **33**, L355–L357.
- Guckenheimer, J. & Holmes, P. [1983] *Nonlinear Oscillations, Dynamical Systems, and Bifurcations of Vector Fields* (Springer-Verlag, NY).
- Jeevarathinam, C., Rajasekar, S. & Sanjuán, M. A. F. [2011] "Theory and numerics of vibrational resonance in Duffing oscillators with time-delayed feedback," *Phys. Rev. E* **83**, 066205-1–12.
- Jeyakumari, S., Chinnathambi, V., Rajasekar, S. & Sanjuán, M. A. F. [2009a] "Analysis of vibrational resonance in a quintic oscillator," *Chaos* **19**, 043128-1–8.
- Jeyakumari, S., Chinnathambi, V., Rajasekar, S. & Sanjuán, M. A. F. [2009b] "Single and multiple vibrational resonance in a quintic oscillator with monostable potentials," *Phys. Rev. E* **80**, 046608-1–8.
- Jeyakumari, S., Chinnathambi, V., Rajasekar, S. & Sanjuán, M. A. F. [2011] "Vibrational resonance in an asymmetric Duffing oscillator," *Int. J. Bifurcation and Chaos* **21**, 275–286.
- Kwuimy, C. K., Nataraj, C. & Litak, G. [2011] "Melnikovs criteria, parametric control of chaos, and stationary chaos occurrence in systems with asymmetric potential subjected to multiscale type excitation," *Chaos* **21**, 043113-1–12.
- Landa, P. S. & McClintock, P. V. E. [2000] "Vibrational resonance," *J. Phys. A: Math. Gen.* **33**, L433–L438.
- Lenci, S. & Rega, G. [2003] "Optimal control of homoclinic bifurcation: Theoretical treatment and practical reduction of safe basin erosion in the Helmholtz oscillator," *J. Vibr. Contr.* **9**, 281–315.
- Medio, A. & Lines, M. [2001] *Nonlinear Dynamics: A Primer* (Cambridge University Press, Cambridge).
- Monje, C. A., Chen, Y., Vinagre, B. M., Xue, D. & Feliu, V. [2010] *Fractional-Order Systems and Controls: Fundamentals and Applications* (Springer, Berlin).
- Oldham, K. B. & Spanier, J. [2002] *The Fractional Calculus: Theory and Applications of Differentiation and Integration to Arbitrary Order* (Dover, Mineola, NY).
- Rajasekar, S., Jeyakumari, S., Chinnathambi, V. & Sanjuán, M. A. F. [2010] "Role of depth and location of minima of a double-well potential on vibrational resonance," *J. Phys. A: Math. Theor.* **43**, 465101-1–11.
- Shang, H. & Xu, J. [2009] "Delayed feedbacks to control the fractal erosion of safe basins in a parametrically excited system," *Chaos Solit. Fract.* **41**, 1880–1896.
- Sun, K., Wang, X. & Sprott, J. C. [2010] "Bifurcations and chaos in fractional-order simplified Lorenz system," *Int. J. Bifurcation and Chaos* **20**, 1209–1219.
- Tcherniak, D. [1999] "The influence of fast excitation on a continuous system," *J. Sound Vibr.* **227**, 343–360.
- Thomsen, J. J. [1999] "Using fast vibrations to quench friction-induced oscillations," *J. Sound Vibr.* **228**, 1079–1102.
- Thomsen, J. J. [2003] *Vibrations and Stability: Advanced Theory, Analysis, and Tools* (Springer, Berlin).
- Wang, J., Cao, L. & Wu, D. [2003] "Effect on the mean first passage time in symmetrical bistable systems by cross-correlation between noises," *Phys. Lett. A* **308**, 23–30.
- Xu, W., Jin, Y. F., Li, W. & Ma, S. J. [2005] "Stochastic resonance in an asymmetric bistable system driven by multiplicative and additive noise," *Chin. Phys.* **14**, 1077–1081.
- Yang, J. H. & Zhu, H. [2012] "Vibrational resonance in Duffing systems with fractional-order damping," *Chaos* **22**, 013112-1–9.
- Yang, J. H., Sanjuán, M. A. F., Xiang, W. & Zhu, H. [2013] "Pitchfork bifurcation and vibrational resonance in a fractional-order Duffing oscillator," *Pramana* **81**, 943–957.
- Yang, J. H. & Zhu, H. [2013] "Bifurcation and resonance induced by fractional-order damping and time delay feedback in a Duffing system," *Commun. Nonlin. Sci. Numer. Simulat.* **18**, 1316–1326.